






Repeated mild traumatic brain injury triggers pathology in asymptomatic C9ORF72 transgenic mice

Aydan Kahriman,¹ James Bouley,¹ Idil Tuncali,² Elif O. Dogan,¹ Mariana Pereira,² Thuyvan Luu,³  Daryl A. Bosco,¹ Samer Jaber,⁴  Owen M. Peters,⁵ Robert H. Brown Jr¹ and  Nils Henninger^{1,6}

Frontotemporal dementia (FTD) and amyotrophic lateral sclerosis (ALS) are fatal neurodegenerative diseases that represent ends of the spectrum of a single disease. The most common genetic cause of FTD and ALS is a hexanucleotide repeat expansion in the *C9orf72* gene. Although epidemiological data suggest that traumatic brain injury (TBI) represents a risk factor for FTD and ALS, its role in exacerbating disease onset and course remains unclear.

To explore the interplay between traumatic brain injury and genetic risk in the induction of FTD/ALS pathology we combined a mild repetitive traumatic brain injury paradigm with an established bacterial artificial chromosome transgenic *C9orf72* (C9BAC) mouse model without an overt motor phenotype or neurodegeneration. We assessed 8–10 week-old littermate C9BAC^{tg/tg} ($n = 21$), C9BAC^{tg/-} ($n = 20$) and non-transgenic ($n = 21$) mice of both sexes for the presence of behavioural deficits and cerebral histopathology at 12 months after repetitive TBI.

Repetitive TBI did not affect body weight gain, general neurological deficit severity, nor survival over the 12-month observation period and there was no difference in rotarod performance, object recognition, social interaction and acoustic characteristics of ultrasonic vocalizations of C9BAC mice subjected to repetitive TBI versus sham injury. However, we found that repetitive TBI increased the time to the return of the righting reflex, reduced grip force, altered sociability behaviours and attenuated ultrasonic call emissions during social interactions in C9BAC mice. Strikingly, we found that repetitive TBI caused widespread microglial activation and reduced neuronal density that was associated with loss of histological markers of axonal and synaptic integrity as well as profound neuronal transactive response DNA binding protein 43 kDa mislocalization in the cerebral cortex of C9BAC mice at 12 months; this was not observed in non-transgenic repetitive TBI and C9BAC sham mice.

Our data indicate that repetitive TBI can be an environmental risk factor that is sufficient to trigger FTD/ALS-associated neuropathology and behavioural deficits, but not paralysis, in mice carrying a *C9orf72* hexanucleotide repeat expansion.

1 Department of Neurology, University of Massachusetts Chan Medical School, Worcester, MA 01605, USA

2 Department of Psychological and Brain Sciences, University of Massachusetts, Amherst, MA 01003, USA

3 Department of Molecular Medicine, University of Massachusetts Chan Medical School, Worcester, MA 01605, USA

4 Department of Pathology, University of Massachusetts Chan Medical School, Worcester, MA 01605, USA

5 School of Biosciences, UK Dementia Research Institute, Cardiff University, Cardiff, CF24 4HQ, UK

6 Department of Psychiatry, University of Massachusetts Chan Medical School, Worcester, MA 01605, USA

Correspondence to: Nils Henninger, MD, PhD, Dr med
Departments of Neurology and Psychiatry, University of Massachusetts Chan Medical School
55 Lake Ave, North, Worcester, MA 01655, USA
E-mail: nils.henninger@umassmed.edu

Keywords: amyotrophic lateral sclerosis; frontotemporal dementia; neurodegeneration; C9orf72; transactive response DNA binding protein 43 kDa (TDP-43)

Introduction

Frontotemporal dementia (FTD) and amyotrophic lateral sclerosis (ALS) are devastating, fatal, progressive neurodegenerative diseases that have no effective treatment. FTD comprises a heterogeneous group of clinical syndromes that are characterized by prominent behavioural changes, executive dysfunction or progressive aphasia.^{1–3} While FTD phenotypes are typically characterized by frontotemporal lobar degeneration, histological features vary.² FTD is the second most common cause of early-onset (<65 years) dementia⁴ with a prevalence of ~15/100 000 population in this age group.⁴ Although the majority of cases have no known cause, more than 30–50% of affected individuals have a family history of FTD,^{5,6} and 10–15% are secondary to autosomal dominant mutations in one of several FTD-associated genes.⁷ ALS is characterized by the degeneration of motor neurons in the brain, brainstem and spinal cord and has a worldwide prevalence of ~5/100 000 population.⁸ In ~15% of ALS patients, neurodegeneration is also observed in the prefrontal and temporal cortex, leading to frontal executive dysfunction, speech production disorders and concurrent FTD.⁹

Because of significant clinical and neuropathological overlap, FTD and ALS represent ends of the spectrum of a single disease. Indeed, a subset of FTD patients develop features of motor neuron disease. Most cases of ALS and the most frequent form of FTD share a pathological hallmark of ubiquitinated inclusions in the cytoplasm of neurons that contain transactive response DNA binding protein 43 kDa (TDP-43); present in ~40–50% of FTD cases.^{3,10} It is now recognized that the most common genetic cause of FTD and ALS (c9FTD/ALS) is a hexanucleotide repeat expansion (HRE) in the chromosome 9 open reading frame 72 (C9orf72) gene and expansion in the gene is always associated with TDP-43 pathology.^{2,6,11,12} While healthy individuals typically have <30 of these repeats, people carrying the mutation can have thousands of repeats.^{7,13} The exact mechanisms by which these expansions cause neurodegeneration are not completely understood. Non-expanded wild-type C9ORF72 interacts with endosomes and is required for normal vesicle trafficking, autophagy induction and lysosomal biogenesis in motor neurons.¹⁴ Presence of HRE has been associated with both impaired transcription, leading to C9ORF72 haploinsufficiency and reduced neuronal viability^{15,16} as well as accumulation of neurotoxic hexanucleotide transcripts and their translation to poly-dipeptides.^{17, 18}

Strikingly, typical pathology has been found to predate disease onset by up to 15 years and disease onset as well as duration are highly variable.^{3,7,19} These observations underscore the concept that environmental stimuli may modulate disease onset and course. In particular, accumulating epidemiological data suggest that traumatic brain injury (TBI) represents a risk factor for FTD/ALS and accelerates disease onset and progression in affected individuals.^{20–24} Indeed, in veterans diagnosed with dementia, the prevalence of TBI history was significantly greater in those with FTD than in those with other types of dementia.²¹ After accounting for pertinent confounders, TBI was associated with an ~4-fold increased risk of FTD.²¹ Nevertheless, not all studies found such a link²⁵ and direct evidence that c9FTD/ALS is mediated by TBI or TBI-related pathology is lacking. Major challenges in unravelling the potential mechanisms by which TBI could cause FTD/ALS

include the fact that many injury-related consequences take years to develop, the pathophysiology of TBI is complex and multiple pathologies overlap between diseases. For example, in both TBI and c9FTD/ALS, pathology includes widespread neuronal degeneration, neuroinflammation, as well as mislocalization and deposition of TDP-43.^{26–30} However, the relationship between these common features in disease progression is poorly understood. It remains to be established whether TBI represents a trigger that could accelerate pathology in at-risk HRE carriers.

Here we explore the interplay between TBI and genetic risk in the induction of c9FTD/ALS pathology by combining a mild repetitive TBI (rTBI) paradigm with a previously established bacterial artificial chromosome transgenic C9orf72 (C9BAC) mouse model. These mice develop no overt motor phenotype and neurodegeneration.³¹ Our data show that rTBI in 3-month-old C9BAC mice causes persistent neuroinflammation and neurodegeneration as well as behavioural deficits that are not observed in non-transgenic (Ntg) and sham-operated control mice.

Materials and methods

All mouse experiments were conducted at The University of Massachusetts Chan Medical School following protocols approved by the Institutional Animal Care and Use Committee. Mice of both sexes were used in all experiments [26 (41.3%) females and 37 (58.7%) males]. Overall, the animals' sex distribution was similar across studied genotypes [C9BAC hemizygous (C9BAC^{tg/-}), 55% male and 45% female; C9BAC homozygous (C9BAC^{tg/tg}), 50% male and 50% female; Ntg, 71.4% male and 28.6% female]. Animals were socially housed in same-sex groups ($n = 4$ per cage) on 12-h light/dark cycle with food and water *ad libitum* in a specific pathogen-free barrier facility. Spontaneously breathing mice ($n = 63$; age 8–10 weeks; 27.1 ± 3.1 g body weight) were randomly subjected to sham surgery ($n = 29$) versus closed head rTBI ($n = 34$). Brains were removed 52 weeks after rTBI for histological analyses.

Animal model

This study used a previously described transgenic mouse model from our laboratory that harbours the human C9ORF72 HRE expressing ~500 repeat motifs within a truncated human C9orf72 gene (from exons 1–6).³¹ Hemizygous mice express three to five copies of the transgene.³¹ We previously showed that the truncated human C9orf72 gene generates three transcript variants of which V1 and V3 carry the repeat expansion. Human-specific probes targeting human C9orf72 V1, V2 and V3 mRNAs detected all three transcripts in the C9BAC mice at expression levels relative to their abundances in human frontal cortex. Further, the total level of the transgenic human transcripts was comparable to that of the endogenous mouse C9orf72 orthologue transcripts and to levels of expression of human control and c9FTD/ALS cases.³¹ Whilst, to our knowledge, c9FTD/ALS patients (with rare exceptions³²) almost exclusively carry a single expanded allele, we included homozygous mice to increase the transgene load. With this approach we sought to increase possible phenotypic penetrance given the short lifespan of mice, which allows for less time for cumulative pathology to

develop, as well as assess for any dose effect. For all experiments, Ntg, hemizygous and homozygous C9ORF72 BAC transgenic mice were used. Hemizygous C9BAC mice (C9BAC^{tg/-}) were viable, producing progeny at expected Mendelian frequencies. Homozygous C9BAC (C9BAC^{tg/tg}) females were not used for breeding due to high rates of maternal infanticide. Mice were generated either by crossing hemizygous with homozygous mice (for homozygous and hemizygous offspring) or by crossing hemizygous mice (for hemizygous and Ntg offspring).

Repeated mild traumatic brain injury model

Animals were anaesthetized with isoflurane (5% for induction, 2% for surgery, 1.5% for maintenance) in room air. Anaesthesia was discontinued immediately prior to each impact and sham injury. Body temperature was monitored continuously with a rectal probe and maintained at $37.0 \pm 0.5^\circ\text{C}$. To alleviate pain, animals received 1.5 mg/kg subcutaneous buprenorphine (Med-Vet International) 30 min before anaesthesia and every 6 h afterwards for 24 h. Additionally, each animal received 5 mg/kg subcutaneous carprofen (Patterson Veterinary) after the start of anaesthesia. A weight drop device was used to produce rTBI as previously described²⁶ with the modification that animals were subjected to rTBI or sham injury once daily for five consecutive days using a 25 g weight. The weight was freely dropped 15 cm to strike a cylindrical polyacetal transducer rod (Delrin[®], tip diameter 2 mm, 17.4 g) that was placed with its tip directly on the exposed skull (target 2.5 mm posterior and 2.5 mm lateral from Bregma). The mouse head was not restrained to allow acceleration upon impact. Following each TBI, the bone was visually inspected under the operating microscope and animals with a skull fracture immediately euthanized without recovering from anaesthesia. The wound was closed with interrupted sutures and the animal returned to its home cage after recovery from anaesthesia. Sham animals were anaesthetized, surgically prepared (including skin incision) and placed under the impact device with the impactor touching the skull but were not subjected to head impact.

Immunohistochemistry

Animals were perfused under anaesthesia through the ascending aorta with 50 ml saline and then with ice cold phosphate-buffered 4% paraformaldehyde (PFA) for 10 min. Brains were removed, post-fixed overnight in the same fixative and then stored in 0.4% PFA at 4°C until further processing. Prior to paraffin embedding brains were pre-sectioned using a brain matrix. For histological assessment paraffin sections, 10- μm thick coronal, were obtained at approximately Bregma -2.5 mm (impact centre), as described.²⁶ All histological analyses were performed by an investigator masked to the animal groups. Immunohistochemistry was performed against TDP-43 (1:250, Proteintech, Cat. No. 10782-2-AP, RRID: AB_615042) neuronal nuclei (NeuN, 1:200, Proteintech, Cat. No. 26975-1-AP, RRID: AB_2880708), Beta-III tubulin (Tuj1, 1:250, BioLegend, Cat. No. 801201, RRID: AB_2313773), glial fibrillary acidic protein (GFAP, 1:250, Agilent, Cat. No. Z0334, RRID: AB_10013382), ionized calcium binding adaptor molecule 1 (Iba-1, 1:250, Wako, Cat. No. 019-19741, RRID: AB_839504), microtubule-associated protein 2 (MAP2, 1:250, Thermo Fisher Scientific, Cat. No. 13-1500, RRID: AB_2533001), pan-axonal anti-neurofilament marker (SMI-312, 1:200, BioLegend Cat. No. 837904, RRID: AB_2566782), postsynaptic density protein 95 (PSD-95, 1:250, Thermo Fisher Scientific, Cat. No. MA1-045, RRID: AB_325399) and synaptophysin

(Synaptophysin, 1:250, Millipore Cat. No. AB9272, RRID: AB_570874). For chromogenic staining, tissue sections labelled with the primary antibodies (NeuN) were incubated with appropriate biotin-conjugated secondary antibodies followed by avidin-biotin complex (Vector Laboratories) incubation and treatment with diaminobenzidine as directed by the manufacturer. For immunofluorescence staining tissue sections labelled with the primary antibodies (TDP-43, NeuN, GFAP, Iba-1, MAP2, SMI-312, synaptophysin, PSD-95) were incubated in appropriate secondary antibodies conjugated with Alexa Fluor 488 (1:250, Abcam, Cat. No. ab150113, RRID: AB_2576208 and Cat. No. ab150077, RRID: AB_2630356), Alexa Fluor 555 (1:250, Abcam, Cat. No. ab150106, RRID: AB_2857373) and Alexa Fluor 647 (1:250, Abcam, Cat. No. ab150075, RRID: AB_2752244 and Cat. No. ab150115, RRID: AB_2687948). Omitting the primary antibody in a subset of slides served as negative controls.

Image acquisition and quantification

To acquire images of all stained sections for subsequent offline analysis we used a Leica DM6 B microscopy system equipped with a brightfield DMC5400 colour CMOS camera and an immunofluorescent DFC9000 sCMOS camera.

For quantitative thresholded area measurements of histological data we used the Analyze Particle tool in ImageJ as described,²⁶ with the experimenter blinded to the genotype and injury. To determine the extent of neuronal loss, chromogen stained NeuN-positive cells were assessed in each coronal section. Images of 16 non-overlapping regions of interest (ROIs; eight per hemisphere; $659 \times 439 \mu\text{m}$, each) covering the dorsal cerebral cortex were taken at $\times 20$ magnification. To assess the impact of rTBI on axonal integrity, we used fluorescence staining for SMI-312 to quantify the signal from two ROIs (one per hemisphere; $659 \times 439 \mu\text{m}$, each). In addition, we manually counted the number of axon profiles in the mid-section of the ROIs used for thresholded SMI-312 signal assessment. To determine pre- and postsynaptic cortical synaptic integrity, we quantified the synaptophysin and PSD-95 staining signal in two ROIs centred within corresponding ROIs used for the SMI-312 analysis (one per hemisphere; $333 \times 333 \mu\text{m}$, each) taken at $\times 40$ magnification. For GFAP, images of two ROIs (one per hemisphere; $667 \times 667 \mu\text{m}$, each) were taken at $\times 20$ magnification. For TDP-43 and Iba-1, images of two ROIs (one per hemisphere; $211 \times 211 \mu\text{m}$, each) centred within the corresponding ROI used for the GFAP analyses were taken at $\times 63$ magnification. Stained regions of confocal images were selected by setting a single common threshold intensity for all images for a particular staining method.

We used Sholl analysis to describe microglial morphology in the ipsilateral cortex stained with Iba-1. The number of intersections of a cell with circles of increasing diameters indicates the degree of ramification of the cell. One ROI per hemisphere ($635.6 \times 635.6 \mu\text{m}$, as taken at $\times 63$ magnification) centred within the corresponding ROI used for the axonal analyses was analysed. Z-stacked confocal images were merged into a single plane image using the LSM Image Browser software (Carl Zeiss Inc.). Five cells were selected randomly per image with the following selection criteria: (i) a cell needed to have a visible soma; (ii) a cell should not overlap with other cells; and (iii) a DAPI-stained nucleus must be clearly visible within the soma. Using ImageJ, images were converted to 8-bit files and a uniform threshold was applied to all images. The Neuroanatomy Simple Neurite Tracer plugin was used to trace processes from the soma.³³ Primary paths were

merged into a shared root and for Sholl and convex hull analyses, paths were converted to binary skeletons. For Sholl analysis, the centre of each Sholl radius was placed at the shared root and concentric circles were placed 0.2 μm apart to detect the number of intersections at each circle. For convex hull analysis, convex hull area was defined as the area of the smallest convex polygon enclosing the entire skeleton.

Behavioural testing

Righting reflex

The return of the righting reflex was defined as the time(s) from discontinuation of anaesthesia to righting from a supine to prone position.

Neurological severity score

The neurological severity score (NSS) was assessed on a scale from 0 (no deficit) to 10 (maximal deficit) prior to rTBI as well as serially until euthanasia, as described.²⁶

Rotarod

Motor function was assessed serially from 3 to 15 months of age (pre-trauma to 52 weeks post-rTBI) using rotarod (Med-Associates Inc.). Mice were tested three times on 4–40 rpm accelerating rotarod task with latency to fall for each individual test recorded. The mean score for each animal was used for statistical analysis.³¹

Grip strength

Limb grip strength was recorded using a digital force gauge (Mark-10) fitted with a metal grid. Mice were placed on the grid, allowing either all paws (all-limb grip strength) to grip or forepaws (forelimb grip strength) only, followed by being gently pulled horizontal to the apparatus until grip was released. Each animal was tested three times for forelimb or all-limb grip, with peak strength for each recorded for statistical analysis.³¹

Novel object recognition

Novel object recognition (NOR) was performed 52 weeks after rTBI using two sample objects with one environment as described with minor modifications.³⁴ First, in the habituation phase, mice were kept for 10 min in a clean, rectangular cage (26 \times 48 \times 23 cm) in a quiet, dimly lit room and then returned to their home cage. On the following day, two identical objects (Object 1 and Object 1') were introduced at opposite corners (in the long-axis) of the cage, approximately 2 cm from the sides. For familiarization, the mice were placed in the cage and allowed to explore the objects for 10 min with the time required to accumulate at least 20 s of orofacial exploration (whisking or sniffing) recorded by the experimenter. At the end of these 10 min, animals were returned to their home cages for 30 min. For the test phase, two different objects were placed in the cage at corners, one object (Object 1) being identical to the previous familiar objects, and one being a novel object (Object 2) of similar size but different colour and shape. Mice were allowed to explore the arena for 5 min in the presence of the familiar and novel objects. The time spent exploring (i.e. nose within 1 cm from the object and/or touching it with the nose and/or forepaws) each object was recorded. The role (familiar or novel), as well as the relative position of the two stimulus objects, was counterbalanced and randomly permuted for each experimental animal. After each trial the objects were discarded, and the cage

cleaned to remove olfactory cues. The total exploration time(s) of each object was recorded to calculate the preference index separately for the familiarization and test phase.

Social motivation and interaction

Social motivation and interaction were evaluated at 12 months after rTBI in the social interaction test as described,^{35,36} with some modifications. This test quantitatively assessed social behaviour in experimental mice shown toward a standard stimulus mouse in a neutral territory. Importantly, this test allows for concomitant measurement of mouse ultrasonic vocalizations (USVs) to assess social and vocal repertoires simultaneously. The testing arena consisted of a clean cage (26 \times 48 \times 23 cm) divided into two equal-sized compartments by a wire mesh. The test consisted of three phases: habituation (Phase A), barrier (Phase B) and interaction (Phase C). After a 5-min habituation period (Phase A), the experimental mice were exposed to a same-sex, unfamiliar, 12-week-old, Ntg stimulus mouse that was introduced behind the wire mesh for 5 min (Phase B). Finally, the barrier was removed and the mice were allowed to interact for 5 min (Phase C). The number of quarter crossings, rearings and self-grooming was recorded separately for each phase and the total number of faecal droppings recorded for Phases A to C combined. During the barrier phase (Phase B), the time spent at the partition was recorded. During direct interaction (Phase C), the number of approaches (frontal versus nose-to-nose), anogenital investigations (stimulus-to-experimental versus experimental-to-stimulus) and close followings (stimulus-to-experimental versus experimental-to-stimulus) was recorded.

Ultrasonic vocalizations

USVs were recorded during the social interaction test using a condenser ultrasound microphone positioned above the testing arena and connected via an UltraSoundGate audio device (Avisoft Bioacoustics) to a computer. Recordings were analysed offline with the Avisoft SASLab Pro signal processing software to assess the test mouse's USV during Phases A–B and the USVs of the pair during Phase C. USV were counted and categorized and the duration, amplitude and peak frequency of each USV measured.

Statistical analysis

Unless otherwise stated, continuous variables are reported as mean \pm standard error of the mean (SEM). Normality of data was examined using the Shapiro–Wilk test. Between-group comparisons were conducted by one-way ANOVA with *post hoc* Holm–Šidák or Tukey test, ANOVA on Ranks with *post hoc* Dunn's test, and Fisher exact test (for USV) with *post hoc* Bonferroni test. Between-group comparisons of continuous variables over repeated measurements (time or ROI) were conducted using longitudinal mixed models. Time/ROI was treated as a categorical variable. The models included group and time/ROI as fixed covariates, as well as the Group \times Time/ROI interactions. When the main effects were significant, additional *post hoc* pairwise comparisons were conducted to isolate significant groups and time points/ROIs with *P*-values adjusted for multiplicity of testing using the false discovery rate (FDR). Survival analysis was conducted by Kaplan Meier analysis and log-rank test. Two-sided significance tests were used and a two-sided *P* < 0.05 was considered statistically significant. All statistical analyses were performed using IBM® SPSS® Statistics Version 26 (IBM®-Armonk, NY).

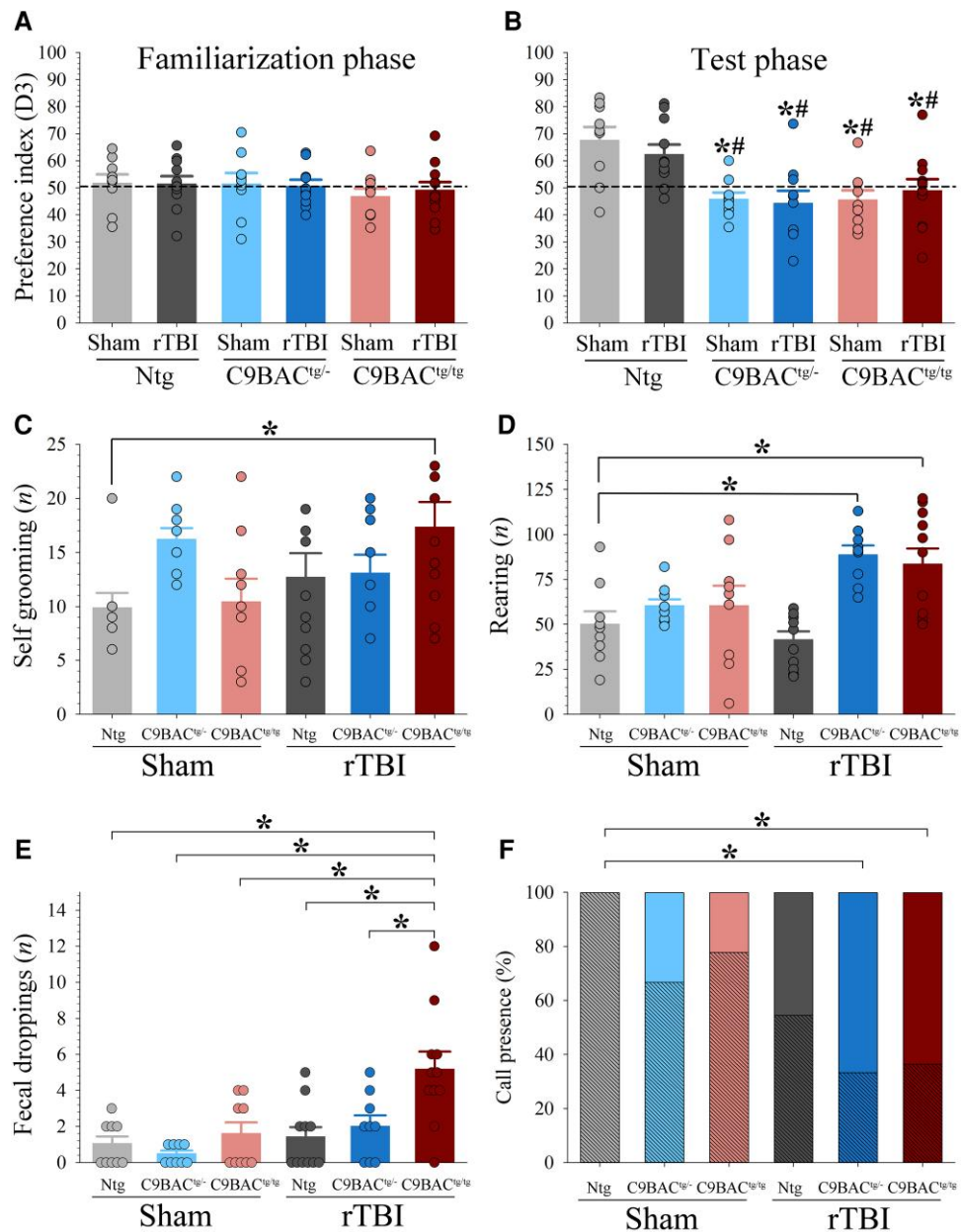


Figure 2 Novel object recognition and social interaction of mice at 12 months after surgery. (A) During the familiarization phase of the novel object recognition test, groups spent an equal percentage of time exploring both objects (dashed line indicates chance performance). (B) During the test phase, both sham operated and rTBI non-transgenic (Ntg) mice spent significantly more time with the novel object. On the contrary, C9BAC hemizygous and homozygous sham and rTBI mice did not discriminate between familiar and novel objects. Between group comparisons were made by one way ANOVA. Data are mean \pm SEM. * $P < 0.05$ versus Ntg sham, # $P < 0.05$ versus Ntg rTBI. (C) Compared to Ntg sham controls, C9BAC^{tg/tg} mice displayed significantly increased self-grooming behaviour. (D) Increased rearing behaviour in C9BAC^{tg/-} and C9BAC^{tg/tg} mice after rTBI as compared to Ntg sham controls. (E) After rTBI C9BAC^{tg/tg} mice showed significantly increased number of faecal droppings when compared to all other groups. Data in A–E were compared by one-way ANOVA with *post hoc* Holm–Šidák test and presented as mean \pm SEM. (F) Significantly fewer C9BAC^{tg/-} and C9BAC^{tg/tg} mice emitted USV at 52 weeks after rTBI compared to non-transgenic (Ntg) sham controls ($P = 0.019$, Fisher’s exact test with *post hoc* Bonferroni adjustment). Hatched bars indicate call presence, open bars indicate call absence. For clarity, only significant results are indicated in the figure.

HRE and rTBI on social dysfunction in our mouse model, we studied social motivation and interaction of experimental mice (C9BAC and wild-type Ntg) with same sex Ntg stimulus mice in a neutral testing cage. We found that rTBI significantly increased self-grooming in C9BAC^{tg/tg} mice when compared to Ntg sham controls (Fig. 2C). In addition, rTBI caused increased rearing behaviour in C9BAC^{tg/-} and C9BAC^{tg/tg} animals (Fig. 2D). Finally, C9BAC^{tg/tg} animals subjected to rTBI showed a greater number of faecal droppings during the test than all other groups (Fig. 2E). Together, changes in these

behaviours may indicate increased stress-induced anxiety-like behaviours^{39–42} in C9BAC^{tg/tg} mice following rTBI.

Regarding social parameters, we found no significant difference between experimental groups in the time spent at the partition (Supplementary Fig. 2A), frequency of quarter crossings (Supplementary Fig. 2B) and total number of direct social interactions (i.e. the sum of close followings, frontal approaches, nose-to-nose and anogenital investigations; Supplementary Fig. 2C). When we stratified the analyses of direct social interaction by

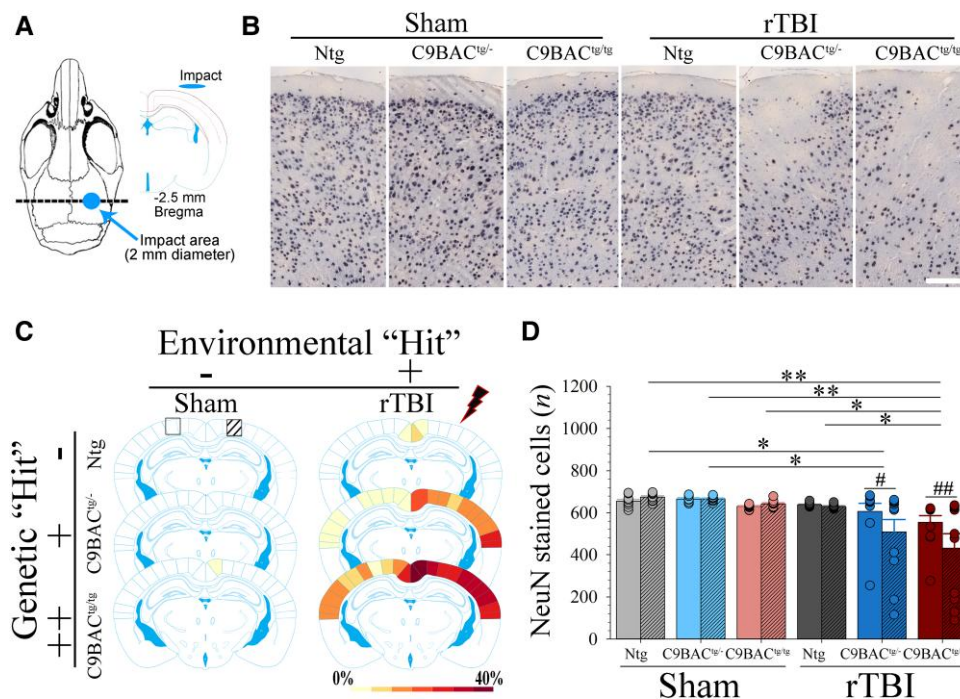


Figure 3 Repetitive TBI causes extensive neuronal loss at 12 months after injury in C9BAC mice. (A) Schematic of the mouse skull denoting the approximate location of the impact centre over the intact mouse skull (blue circle) as well as (B) relative to the brain section sampled for histological analysis shown in this figure (dashed line). (C) Loss of NeuN stained neurons in the cerebral cortex of C9BAC^{tg/-} and C9BAC^{tg/tg} mice after rTBI (images were taken from an area corresponding to the striped square in C). Scale bar = 120 μ m. (C) Cartoon depicting the extent of neuronal loss within the conceptual framework that the combined risk of rTBI (environmental 'hit') and C9orf72 gene mutation (genetic 'hit') cause neuronal loss [– risk absent (Ntg sham mice), + or ++ risk present (C9BAC^{tg/-} or C9BAC^{tg/tg} mice with or without rTBI)]. Data are expressed as % reduction [range 0% (white) to 40% (red)] relative to the corresponding region of interest in Ntg sham mice (lightning bolt denotes the site of impact delivery). Squares indicate the approximate ROI used for quantitative analyses shown in D. (D) Significant reduction in the number of NeuN stained neurons at 12 months after rTBI in C9BAC^{tg/-} and C9BAC^{tg/tg} mice, with overall greater neuronal loss in the ipsilateral versus contralateral hemisphere ($P < 0.001$ for group effect, $P = 0.014$ for left versus right ROI, $P = 0.005$ for Group \times ROI interaction). For each genotype, data on the right are from the ipsilateral cortex. Data in the bar graph are shown as mean \pm SEM. $n = 9$ –12 per group. * $P < 0.05$, *** $P < 0.001$ for between group comparisons; # $P < 0.05$, ### $P < 0.001$ for between hemisphere comparisons (post hoc pairwise comparisons FDR adjusted).

the individual parameters, we found no significant between-group difference in the individual behavioural components of direct social interaction (Supplementary Fig. 3A–F). No aggression was observed in interactions between experimental and stimulus mice.

Repetitive TBI reduces the emission calls of C9BAC mice during social interactions

Mice emit a diverse repertoire of communicative vocalizations in the ultrasonic range. USVs have a frequency range between 30 and 110 kHz and serve important communicative functions, for example, to establish social contacts with conspecifics.⁴³ USVs are increasingly used as a valuable tool to inform on deficits in communication and sociability in a variety of murine models of neurological disease including TBI and neurodegenerative conditions.^{44–47} To determine potential deficits in social communication as a result of rTBI, USVs were simultaneously recorded during the social interaction test. We observed a highly skewed distribution of USVs ranging from 0 to 944 with no calls recorded in 19 tests (32.8%). Not all animals emitted USVs during each phase of the social interaction test. While there was no difference in the USV acoustic parameters, including the frequency, amplitude and duration of the recorded calls between groups (Supplementary Fig. 4A–C), we found that after rTBI, significantly fewer C9BAC^{tg/-} and C9BAC^{tg/tg} mice emitted calls compared to Ntg sham controls (Fig. 2F).

Repetitive TBI causes extensive neuronal loss at 12 months after injury in C9BAC mice

Having established changes in motor performance in the C9BAC mice exposed to rTBI, we next used histological staining to assess for a possible impact on cerebral integrity. At 12 months after rTBI we found a striking loss of neuronal density in the cerebral cortex of C9BAC mice that was not observed in Ntg rTBI and sham mice (Fig. 3). Loss of NeuN positive cells in C9BAC mice was most pronounced within the ipsilateral cerebral cortex underlying the impact centre (Bregma -2.5 mm), with less neuronal loss in the contralateral unimpacted hemisphere (Fig. 3C and D). Although C9BAC^{tg/-} mice had numerically fewer intact neurons than C9BAC^{tg/tg} mice, this difference did not reach statistical significance. Because neurons may retain their cellular integrity despite loss of NeuN immunoreactivity under specific conditions (such as ischaemia), we also used the neuron-specific marker Tuj1 to confirm our findings. Similar to the loss of NeuN immunoreactivity, we found a significant reduction of Tuj1 staining in C9BAC^{tg/-} and C9BAC^{tg/tg} mice after rTBI (Supplementary Fig. 5)

Repetitive TBI accentuates loss of SMI-312 stained axon profiles at 12 months after injury in C9BAC mice

Having established that rTBI accentuates neuronal loss in our model, we next sought to determine the possible impact on axonal

integrity as axonal injury and degeneration are pathological hallmarks of TBI and FTD/ALS.⁴⁸ While other mouse models expressing the human C9orf72 repeat and/or dipeptide repeats showed peripheral axonal loss^{31,49,50} it was not previously known whether C9orf72 transgenic mouse models replicate cerebral axon loss or if TBI accentuates this pathology. We found that 12 months after surgery (age ~15 months) sham operated C9BAC^{tg/-} and C9BAC^{tg/tg} mice exhibited a significant loss of cortical staining for the pan-neurofilament marker SMI-312 compared to Ntg controls. Similarly, there was a significant reduction in the number of SMI-312 stained axon profiles. This axonal pathology was significantly accentuated by rTBI, whereby the reduction in cortical SMI-312 stained axon profiles was more pronounced in the ipsilateral versus contralateral hemisphere of C9BAC mice (Fig. 4A–C).

Repetitive TBI accentuates loss of cortical synaptic proteins at 12 months after injury in C9BAC mice

Several lines of data indicate that progressive synapse loss and synaptic dysfunction occur in FTD and ALS⁵¹ and mounting evidence indicates that TBI-induced axonal loss is accompanied by synaptic pathology.⁵² However, it is presently uncertain whether TBI contributes to persistent synaptopathy in c9FTD/ALS. Thus, we sought to determine whether rTBI affects synaptic integrity in the cerebral cortex C9BAC mice. We found that 12 months after surgery sham operated C9BAC^{tg/-} and C9BAC^{tg/tg} mice exhibited a significant reduction the postsynaptic marker PSD-95 as well as the presynaptic marker synaptophysin within the cerebral cortex when compared to Ntg controls. This synaptic pathology was significantly accentuated by rTBI (Fig. 4D and E).

Prominent TDP-43 mislocalization at 12 months after repetitive TBI in C9BAC mice

Persistent or irreversible cytoplasmic accumulation of TDP-43 is a major pathological event in tau-negative cases of FTD¹⁰ as well as in several other TBI-associated degenerative diseases. TDP-43 is a promiscuous binding protein that interacts with many different RNA, DNA and protein targets.^{53,54} Under physiological conditions, it is mainly localized in the nucleus, but a small proportion of TDP-43 is located in the cytoplasm, where it binds mature mRNA, participating in the regulation of the stability, transport translation and splice surveillance of mRNA. After neuronal injury, TDP-43 is mislocalized to the cytoplasm.^{54,55} Interestingly, in animal models of FTD/ALS, TDP-43 mislocalization has been shown to adversely affects synaptic integrity⁵⁶ and it is increasingly recognized that TBI can cause widespread TDP-43 mislocalization.²⁶ In light of our observation that rTBI accentuated loss of the axonal marker SMI-312 as well as the synaptic markers PSD-95 and synaptophysin, we sought to determine whether rTBI caused TDP-43 mislocalization in C9BAC mice. Concurrent with the neuronal loss at 12 months after rTBI we noted an overall reduction in TDP-43 staining signal in the cerebral cortex of C9BAC mice that was not present in Ntg rTBI and C9BAC sham controls (Fig. 5A and B). On a cellular level, we found that ~80% of all NeuN stained neurons expressed TDP-43 without a significant difference between the experimental groups (Fig. 5C). Further, the C9BAC mice without trauma did not exhibit neuronal TDP-43 mislocalization at 12 months after sham procedure (~15 months old), nor did they reveal a change in the overall number of TDP-43 stained neurons (compared to Ntg controls). Likewise, Ntg rTBI mice showed normal nuclear TDP-43 staining (Fig. 5A and B). In contrast, C9BAC mice exhibited a

prominent loss of nuclear TDP-43 with cytoplasmic mislocalization and inclusions in both the ipsilateral as well as contralateral cerebral cortex at 12 months after rTBI (Fig. 5A and D). Strikingly, the proportion of cells showing TDP-43 mislocalization in the ipsilateral hemisphere was significantly greater in C9BAC^{tg/tg} versus C9BAC^{tg/-} mice (44.2 ± 8.7% versus 16.7 ± 4.6%) (Fig. 5D).

Repetitive TBI promotes widespread microglial but not astroglial activation in C9BAC mice

Microglial activation has been found in human c9FTD/ALS post-mortem brains, as evidenced by altered cell morphology and increased expression of Iba1 and CD68 compared to sporadic FTD/ALS cases.^{27,28,57} We found that in our model C9BAC^{tg/-} and C9BAC^{tg/tg} mice had significantly increased Iba-1 staining signal in the cerebral cortex at 12 months after rTBI that was not observed in Ntg rTBI and sham controls (Fig. 6A and B) without corresponding astroglial activation (Fig. 6C). Morphological analysis demonstrated widespread microglial activation in rTBI mice as indicated by the presence of a hyper-ramified morphology (Fig. 6A), increased convex hull area (Fig. 6D) and increased number of process intersections per Sholl radius (Fig. 6E).

Discussion

The environmental factors that could increase susceptibility to FTD/ALS are poorly understood. Several epidemiological studies have linked a history of TBI to FTD/ALS, particularly in individuals with a history of repeated injuries.^{20–24} Nevertheless, not all studies found such a link and some reported that the association between ALS and TBI was strongest among individuals with head injury within a year from ALS onset, raising concerns of potential reverse causation (e.g. a fall-related TBI was caused by weakness in undiagnosed ALS).^{25,58} We now show for the first time that mild rTBI causes profound neuronal and axonal loss and neuroinflammation, with accompanying TDP-43 mislocalization and behavioural deficits in asymptomatic transgenic mice that harbour a portion of the human C9orf72 gene with an expanded GGGGCC repeat motif at 1 year after injury. This is an important observation because these pathologies are common features in both TBI and most cases of FTD/ALS^{26–30,59}; yet, experimental evidence for a direct link has been lacking.

Intriguing insight into the potential links between extrinsic injury and FTD/ALS stem from observations using a *Drosophila* trauma model. Wild-type flies exposed to trauma were shown to have a reduced lifespan and to develop cerebral vacuolar lesions as well as stress granules that are associated with an early accumulation of the TDP-43 homologue TBPH that subsides by 24 h after injury.^{60–62} Flies overexpressing mutations in FUS or C9orf72 in neurons that were exposed to this trauma exhibited increased mortality, exaggerated locomotor deficits and increased formation of ubiquitinated and Ref(2)P-positive (p62) stress granules in the brain.⁶⁰ To what extent these observations extend to mammalian TBI, specifically in the context of FTD/ALS-associated gene deficits, is unknown. In particular, these fly studies did not examine whether the used injury paradigm causes neuronal and axonal loss.^{60,62} It remains to be shown whether injury can indeed accentuate TDP-43 pathology and neurodegeneration in individuals with an at-risk genetic background of FTD/ALS.⁶⁰

Some studies have examined the potential impact of TBI on disease progression in rodent models of ALS that overexpress mutant, human G93A-superoxide dismutase-1 (hSOD1^{G93A}).^{63–67} While a

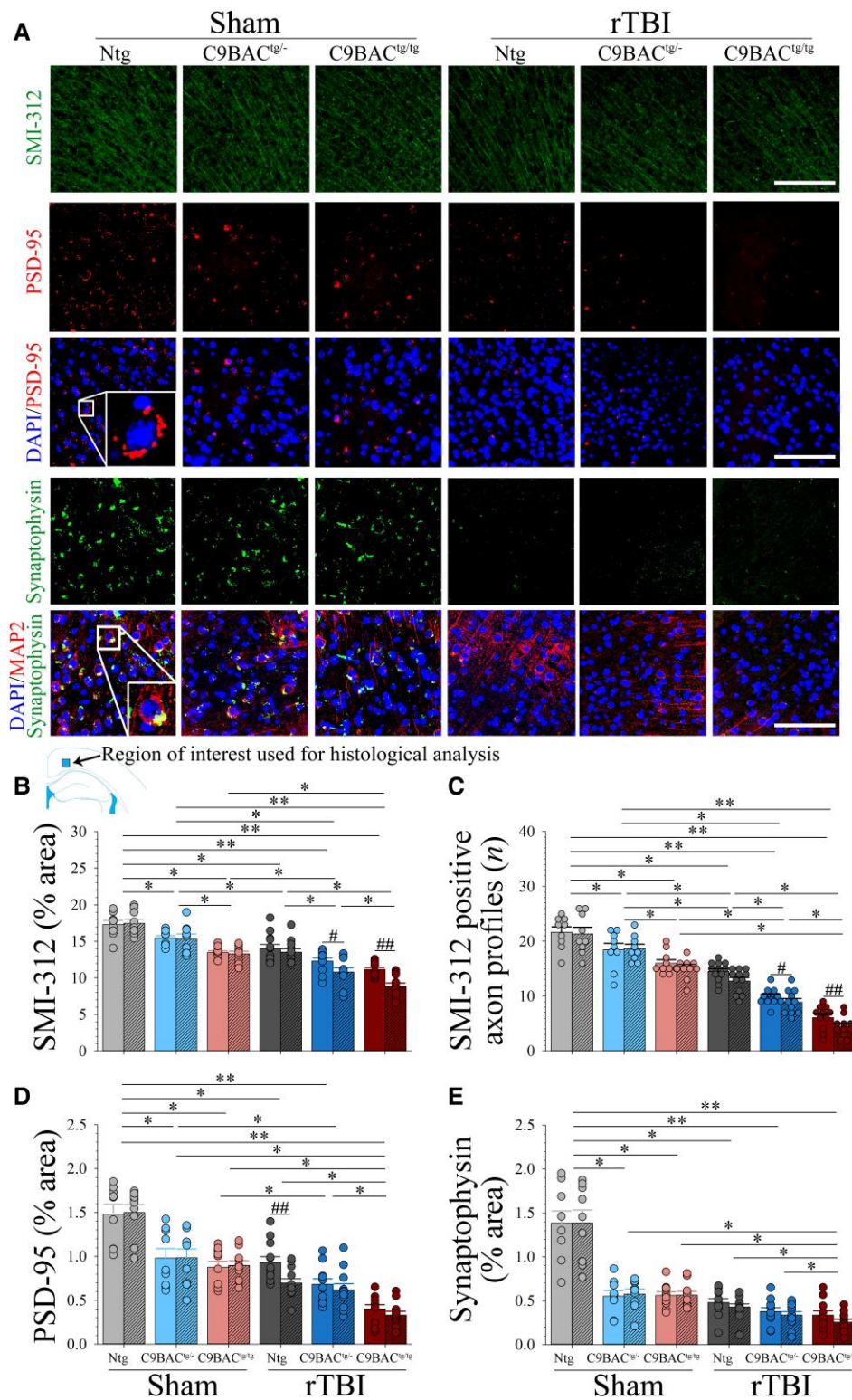


Figure 4 Repetitive TBI accentuates axonal and synaptic loss at 12 months in C9BAC mice. (A) Representative photomicrographs showing SMI-312, PSD-95 and synaptophysin staining signal from the ipsilateral cerebral cortex (square box in inset). Scale bars = 100 μ m. Reduced cortical axonal density in C9BAC mice that is accentuated by rTBI as indicated by (B) attenuated SMI-312 staining signal ($P < 0.001$ for group effect, $P < 0.001$ for left versus right ROI, $P = 0.010$ for Group \times ROI interaction) as well as (C) reduced number of SMI-312 stained axons profiles ($P < 0.001$ for group effect, $P = 0.003$ for left versus right ROI, $P = 0.345$ for Group \times ROI interaction). RTBI accentuates synaptic loss in C9BAC mice as indicated by a reduction in the (D) postsynaptic marker PSD-95 ($P < 0.001$ for group effect, $P = 0.008$ for left versus right ROI, $P = 0.055$ for Group \times ROI interaction) and (E) presynaptic marker synaptophysin ($P < 0.001$ for group effect, $P = 0.004$ for left versus right ROI, $P = 0.940$ for Group \times ROI interaction). Bar-pairs denote left (contralateral) and right (hatched, ipsilateral) ROI. Data are mean \pm SEM. $n = 9$ –12 per group. * $P < 0.05$, ** $P < 0.01$, *** $P < 0.001$ for between group comparisons; ## $P < 0.01$, ### $P < 0.001$ for between hemisphere comparisons (all *post hoc* pairwise comparisons FDR adjusted).

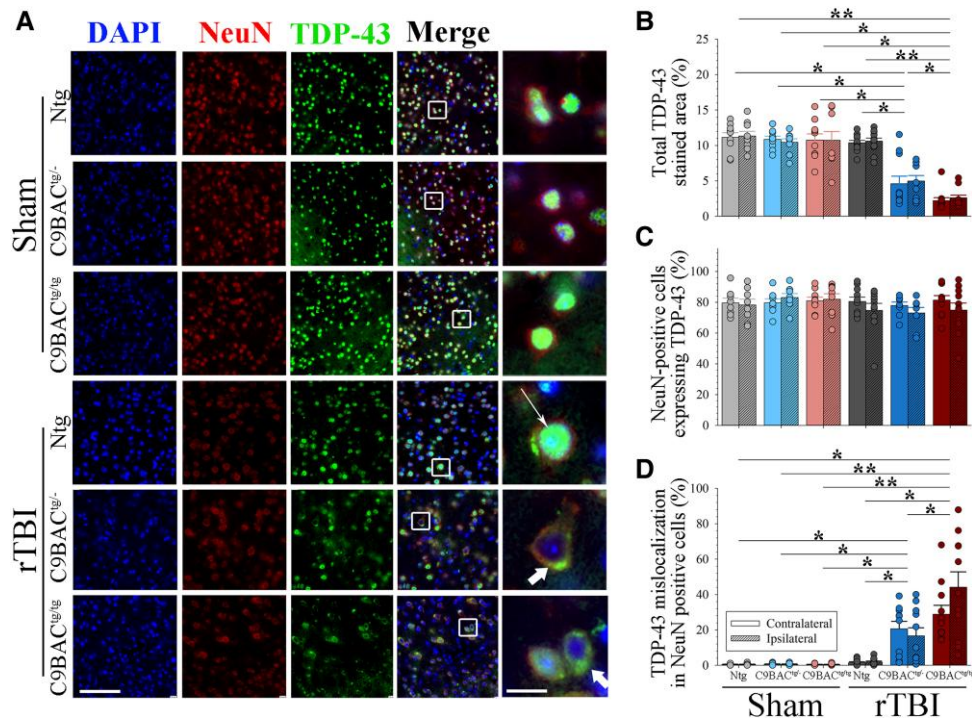


Figure 5 Repetitive TBI causes neuronal TDP-43 mislocalization and accumulation at 12 months in C9BAC mice. (A) Representative photomicrographs showing TDP-43 staining signal from the ipsilateral cerebral cortex. Nuclear localization of TDP-43 in C9BAC sham and non-transgenic (Ntg) rTBI mice (long arrow) at 12 months after rTBI. Nuclear loss and inclusions of cytoplasmic localized neuronal TDP-43 in C9BAC^{tg/-} and C9BAC^{tg/tg} mice (short arrows). Scale bars = 70 μ m. (B) Quantified TDP-43 signal from ROIs corresponding to those used for NeuN staining shows a significant reduction in signal intensity of TDP-43 in both the ipsilateral injured (hatched bars) and contralateral non-injured cortex underlying the impact centre at 12 months after rTBI in C9BAC^{tg/-} and C9BAC^{tg/tg} mice ($P < 0.001$ for group effect, $P = 0.659$ for left versus right ROI, $P = 0.976$ for Group \times ROI interaction). (C) Similar percentage of all NeuN stained neurons expressing TDP-43 between the experimental groups ($P = 0.606$ for group effect, $P = 0.208$ for left versus right ROI, $P = 0.532$ for Group \times ROI interaction). (D) Significantly increased proportion of neurons exhibiting TDP-43 mislocalization in C9BAC^{tg/-} and C9BAC^{tg/tg} mice that is not observed in Ntg rTBI and sham controls ($P < 0.001$ for group effect, $P = 0.816$ for left versus right ROI, $P = 0.691$ for Group \times ROI interaction). Data are mean \pm SEM. $n = 9$ –12 per group. * $P < 0.05$, ** $P < 0.01$, *** $P < 0.001$ for between group comparisons (post hoc pairwise comparisons FDR adjusted).

single TBI did not affect disease onset or mortality in adult hSOD1^{G93A} rats and mice,^{64,65} earlier onset of motor deficits and overall decreased survival were observed in neonate (P7) hSOD1^{G93A} mice after a single closed skull TBI.⁶⁷ Conversely, repetitive mild closed skull TBI was associated with a faster decline in body weight⁶⁶ and earlier onset of motor deficits⁶³ in adult hSOD1^{G93A} rats. However, these studies have several limitations. Although murine hSOD1^{G93A} models have been instrumental in defining the pathobiology of ALS, the hSOD1^{G93A} mutation is a comparatively rare ALS mutation in humans.⁶⁸ Accordingly, it is uncertain to what extent the observed interaction between TBI and hSOD1^{G93A} pathology translates to other FTD/ALS-associated gene mutations, which encode proteins implicated in a wide range of cellular processes that may drive neurodegeneration through a different mechanism than the hSOD1^{G93A} mutation. More important, not all of the above murine hSOD1^{G93A} models conducted detailed histopathological analyses after TBI; none demonstrated that TBI accentuated cortical neuropathology when compared to Ntg TBI animals.^{63,65} In those cases, it is possible that the described TBI-related behavioural dysfunction and mortality were driven by non-specific mechanisms. For example, TBI may result in weight loss that adversely impacts functional performance and increases mortality without affecting neuropathology.⁶⁹

We now show that the interaction between multiple mild head injuries dramatically enhances the initiation of a neurodegenerative process over an extended follow-up time in mice with an

FTD/ALS risk genotype, providing support for the notion that rTBI is sufficient to exaggerate long-term phenotypes and neuropathology associated with FTD/ALS-causing genes in the mammalian brain. We found that rTBI caused persistent microglial activation in our C9BAC model, suggesting that microglia are unable to return to their homeostatic state after a relatively mild exogenous injury. This is an important observation because it is now evident that neurodegeneration at least partially reflects adverse interactions with non-neuronal cells such as microglia.²⁸ Indeed, limited data indicate that glial activation may precede neurodegeneration in FTD/ALS, including TDP-43 mislocalization and accumulation.⁷⁰ For example, disease-causing mutations in microglia promote TDP-43 aggregation and cell death, suggesting that TDP-43 proteinopathy and neurodegeneration in FTD are interlinked with chronic microglial activation.⁷¹ Microglial activation has been found in FTD/ALS patients,^{27–29,57} but the contribution to different disease processes is currently not well delineated. Finally, persistent or irreversible cytoplasmic accumulation of TDP-43 is a major pathological event in tau-negative cases of FTD¹⁰ and a direct relation between TDP-43 and axon biology has recently been defined through the important observation that TDP-43 is essential for the normal splicing and function of stathmin-2.^{72–74} Intriguingly, the magnitude of TDP-43 and synaptic marker staining loss in C9BAC mice was similar in both hemispheres at 1 year. In contrast, the extent of neuronal and axonal loss was significantly greater in the injured hemisphere. This suggests that TDP-43 and synaptic

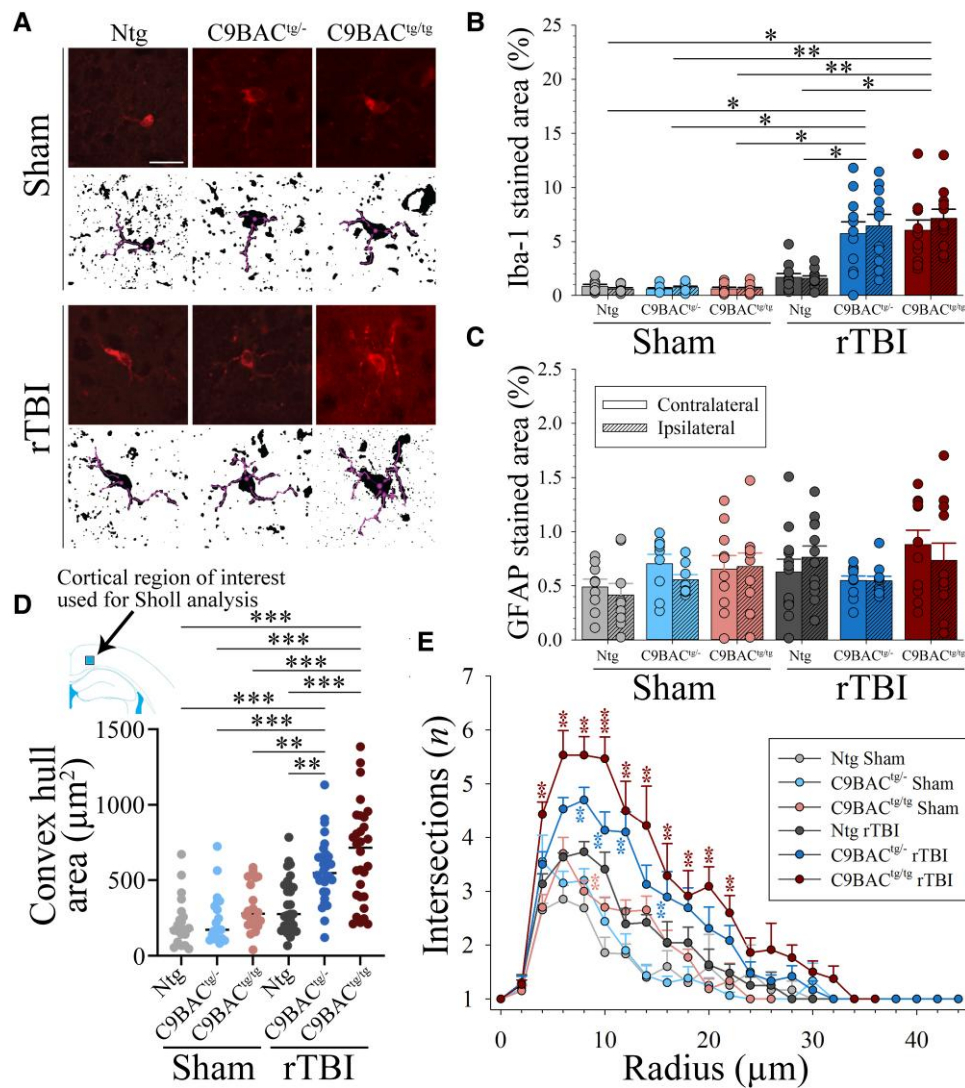


Figure 6 Persistent microglial activation in C9BAC mice at 12 months after repetitive TBI. (A) Representative photomicrographs of Iba-1 stained microglia with corresponding outline used for Sholl analysis. (B) At 12 months after rTBI, C9BAC mice exhibited a significant increase in the number of Iba-1 stained cells in both the ipsilateral injured (hatched bars) and contralateral non-injured cortex underlying the impact centre ($P < 0.001$ for group effect, $P = 0.471$ for left versus right ROI, $P = 0.870$ for Group \times ROI interaction) without (C) corresponding astroglial activation ($P < 0.124$ for group effect, $P = 0.429$ for left versus right ROI, $P = 0.404$ for Group \times ROI interaction). (D) Sholl analysis conducted in the ipsilateral cortex (highlighted by blue square in top diagram) indicated significant enlargement and (E) ramification of microglia of C9BAC mice after rTBI. Scale bar = 10 μm . Data are mean \pm SEM. $n = 9\text{--}12$ per group except $n = 4$ per sham groups and $n = 6$ per for TBI groups for Sholl analysis. * $P < 0.05$, ** $P < 0.01$, *** $P < 0.001$ for between group comparisons in B–D and versus Ntg rTBI in E (post hoc pairwise comparisons were adjusted using Tukey's test in D and the FDR in B, C and E). For clarity, only significant results are indicated in the figure.

pathology precede neuronal and axonal degeneration. Our model is well suited to further dissect the specific links between microglial activation, TDP-43 mislocalization and neuronal degeneration after rTBI in murine HRE carriers.

In addition to the striking rTBI-induced neuropathology, injured C9BAC mice displayed significant behavioural alterations. Specifically, rTBI caused a reduction in limb function, altered sociability behaviours that have been associated with increased stress and anxiety-like behaviours,^{39–42} as well as reduced USV emissions at 12 months, findings that were not present in uninjured control C9BAC mice. Interestingly, these observations are consistent with the reported motor deficits and anxiety-like behaviour described in a different C9BAC mouse model containing the full-length C9orf72 gene with substantial flanking sequence to drive expression of sense and antisense transcripts.⁴⁹ Nevertheless, one limitation of our study is that we lack human data.

While murine models may mimic many important aspects of human disease, they cannot fully replicate the full clinical and pathological spectrum of c9FTD/ALS. Further, although we found that injured C9BAC mice displayed behaviours that mimic some of the phenotypes observed in human c9FTD/ALS,^{1–3,37,38} a direct extrapolation of murine behavioural dysfunction to the human condition is not possible. Moreover, further study is required to both determine whether rTBI promotes the formation of RNA foci and toxic aggregates of repeat-associated non-AUG (RAN) translated poly-dipeptides as well as to resolve their relation to neuropathology and behavioural dysfunction in this model. A better understanding of these relationships may aid the development of novel therapeutic approaches aimed at blocking C9orf72 HRE associated pathology. While such treatments might primarily target c9FTD/ALS^{75,76} it is conceivable that they could also be utilized to more broadly treat TBI. As above, TDP-43 proteinopathy is

common in TBI and several TBI-associated neurodegenerative diseases including c9FTD/ALS and thought to represent an important driver of neurodegeneration. Indeed, alleviating TDP-43 pathology reduced neuronal loss in mice carrying a C9orf72 HRE⁷⁷ and blocking calpain-2 in Ntg mice subjected to rTBI resulted in attenuation of both TDP-43 pathology and axonal loss⁷⁸ suggesting that targeting TDP-43 pathology could reduce neuronal injury after TBI.

In summary, our data support the concept that rTBI is sufficient to trigger FTD/ALS-like neuropathology and behavioural deficits in mice carrying a C9orf72 HRE. Our model provides an important tool both to further dissect the molecular mechanisms by which rTBI drives pathology in this complex disease and to test potential therapeutic strategies for both c9FTD/ALS as well as TBI.

Data availability

All relevant data are included within this manuscript and the [Supplementary material](#). Raw data will be made available on request by qualified researchers.

Funding

This study was supported by NIH/NINDS K08NS091499, R21NS131756 (N.H.), the Riccio Fund for the Neurosciences (N.H., S.J., M.P.) and the Angel Fund for ALS Research (N.H.). N.H. and D.A.B. received support from CDMRP/DoD DOD/W81XWH-20-1-0271. O.M.P. was funded by the UK Medical Research Foundation (MC_PC_16030/2 and MR/W004879/1) and supported by the UK Dementia Research Institute. R.H.B. received support from NINDS NS088689, R01 NS111990, R01 NS104022, the ALS Association, the Angel Fund for ALS Research, the Pierre L. de Bourgnecht ALS Research Foundation, ALS Finding A Cure, ALSOne, the Cellucci Fund, and the Max Rosenfeld ALS Research Fund. The content is solely the responsibility of the authors and does not necessarily represent the official views of the National Institutes of Health.

Competing interests

The authors report no competing interests.

Supplementary material

[Supplementary material](#) is available at *Brain* online.

References

- Ng AS, Rademakers R, Miller BL. Frontotemporal dementia: A bridge between dementia and neuromuscular disease. *Ann N Y Acad Sci*. 2015;1338:71-93.
- Boeve BF, Boxer AL, Kumfor F, Pijnenburg Y, Rohrer JD. Advances and controversies in frontotemporal dementia: Diagnosis, biomarkers, and therapeutic considerations. *Lancet Neurol*. 2022;21:258-272.
- Burrell JR, Halliday GM, Kril JJ, et al. The frontotemporal dementia-motor neuron disease continuum. *Lancet*. 2016;388:919-931.
- Ratnavalli E, Brayne C, Dawson K, Hodges JR. The prevalence of frontotemporal dementia. *Neurology*. 2002;58:1615-1621.
- Blauwendraat C, Wilke C, Simon-Sanchez J, et al. The wide genetic landscape of clinical frontotemporal dementia: Systematic combined sequencing of 121 consecutive subjects. *Genet Med*. 2017;20:240-249.
- Majounie E, Renton AE, Mok K, et al. Frequency of the C9orf72 hexanucleotide repeat expansion in patients with amyotrophic lateral sclerosis and frontotemporal dementia: A cross-sectional study. *Lancet Neurol*. 2012;11:323-330.
- Woollacott IO, Rohrer JD. The clinical spectrum of sporadic and familial forms of frontotemporal dementia. *J Neurochem*. 2016;138 Suppl 1:6-31.
- Rowland LP, Shneider NA. Amyotrophic lateral sclerosis. *N Engl J Med*. 2001;344:1688-1700.
- Phukan J, Elamin M, Bede P, et al. The syndrome of cognitive impairment in amyotrophic lateral sclerosis: A population-based study. *J Neurol Neurosurg Psychiatry*. 2012;83:102-108.
- Mackenzie IR, Rademakers R, Neumann M. TDP-43 and FUS in amyotrophic lateral sclerosis and frontotemporal dementia. *Lancet Neurol*. 2010;9:995-1007.
- DeJesus-Hernandez M, Mackenzie IR, Boeve BF, et al. Expanded GGGGCC hexanucleotide repeat in noncoding region of C9ORF72 causes chromosome 9p-linked FTD and ALS. *Neuron*. 2011;72:245-256.
- Renton AE, Majounie E, Waite A, et al. A hexanucleotide repeat expansion in C9ORF72 is the cause of chromosome 9p21-linked ALS-FTD. *Neuron*. 2011;72:257-268.
- van Blitterswijk M, DeJesus-Hernandez M, Niemantsverdriet E, et al. Association between repeat sizes and clinical and pathological characteristics in carriers of C9ORF72 repeat expansions (Xpansize-72): A cross-sectional cohort study. *Lancet Neurol*. 2013;12:978-988.
- Smeyers J, Banchi EG, Latouche M. C9ORF72: What it is, what it does, and why it matters. *Front Cell Neurosci*. 2021;15:661447.
- Shi Y, Lin S, Staats KA, et al. Haploinsufficiency leads to neurodegeneration in C9ORF72 ALS/FTD human induced motor neurons. *Nat Med*. 2018;24:313-325.
- Zhu Q, Jiang J, Gendron TF, et al. Reduced C9ORF72 function exacerbates gain of toxicity from ALS/FTD-causing repeat expansion in C9orf72. *Nat Neurosci*. 2020;23:615-624.
- Gendron TF, Belzil VV, Zhang YJ, Petrucelli L. Mechanisms of toxicity in C9FTLD/ALS. *Acta Neuropathol*. 2014;127:359-376.
- Pasniceanu IS, Atwal MS, Souza CDS, Ferraiuolo L, Livesey MR. Emerging mechanisms underpinning neurophysiological impairments in C9ORF72 repeat expansion-mediated amyotrophic lateral sclerosis/frontotemporal dementia. *Front Cell Neurosci*. 2021;15:784833.
- Lehmer C, Oeckl P, Weishaupt JH, et al. Poly-GP in cerebrospinal fluid links C9orf72-associated dipeptide repeat expression to the asymptomatic phase of ALS/FTD. *EMBO Mol Med*. 2017;9:859-868.
- LoBue C, Wilmoth K, Cullum CM, et al. Traumatic brain injury history is associated with earlier age of onset of frontotemporal dementia. *J Neurol Neurosurg Psychiatry*. 2016;87:817-820.
- Kalkonde YV, Jawaid A, Qureshi SU, et al. Medical and environmental risk factors associated with frontotemporal dementia: A case-control study in a veteran population. *Alzheimers Dement*. 2012;8:204-210.
- Schmidt S, Kwee LC, Allen KD, Oddone EZ. Association of ALS with head injury, cigarette smoking and APOE genotypes. *J Neurol Sci*. 2010;291(1-2):22-29.
- Chen H, Richard M, Sandler DP, Umbach DM, Kamel F. Head injury and amyotrophic lateral sclerosis. *Am J Epidemiol*. 2007;166:810-816.
- Pupillo E, Poloni M, Bianchi E, et al. Trauma and amyotrophic lateral sclerosis: A European population-based case-control study from the EURALS consortium. *Amyotroph Lateral Scler Frontotemporal Degener*. 2018;19(1-2):118-125.

25. Turner MR, Abisgold J, Yeates DG, Talbot K, Goldacre MJ. Head and other physical trauma requiring hospitalisation is not a significant risk factor in the development of ALS. *J Neurol Sci.* 2010; 288(1–2):45–48.
26. Kahriman A, Bouley J, Smith TW, Bosco DA, Woerman AL, Henninger N. Mouse closed head traumatic brain injury replicates the histological tau pathology pattern of human disease: Characterization of a novel model and systematic review of the literature. *Acta Neuropathol Commun.* 2021;9:118.
27. Bright F, Werry EL, Dobson-Stone C, et al. Neuroinflammation in frontotemporal dementia. *Nat Rev Neurol.* 2019;15:540–555.
28. Beers DR, Appel SH. Immune dysregulation in amyotrophic lateral sclerosis: Mechanisms and emerging therapies. *Lancet Neurol.* 2019;18:211–220.
29. Shao F, Wang X, Wu H, Wu Q, Zhang J. Microglia and neuroinflammation: Crucial pathological mechanisms in traumatic brain injury-induced neurodegeneration. *Front Aging Neurosci.* 2022;14:825086.
30. Bieniek KF, Cairns NJ, Cray JF, et al. The second NINDS/NIBIB consensus meeting to define neuropathological criteria for the diagnosis of chronic traumatic encephalopathy. *J Neuropathol Exp Neurol.* 2021;80:210–219.
31. Peters OM, Cabrera GT, Tran H, et al. Human C9ORF72 hexanucleotide expansion reproduces RNA foci and dipeptide repeat proteins but not neurodegeneration in BAC transgenic mice. *Neuron.* 2015;88:902–909.
32. Fratta P, Poulter M, Lashley T, et al. Homozygosity for the C9orf72 GGGGCC repeat expansion in frontotemporal dementia. *Acta Neuropathol.* 2013;126:401–409.
33. Arshadi C, Gunther U, Eddison M, Harrington KIS, Ferreira TA. SNT: A unifying toolbox for quantification of neuronal anatomy. *Nat Methods.* 2021;18:374–377.
34. Bevins RA, Besheer J. Object recognition in rats and mice: A one-trial non-matching-to-sample learning task to study 'recognition memory'. *Nat Protoc.* 2006;1:1306–1311.
35. Lumley LA, Charles RF, Charles RC, Hebert MA, Morton DM, Meyerhoff JL. Effects of social defeat and of diazepam on behavior in a resident-intruder test in male DBA/2 mice. *Pharmacol Biochem Behav.* 2000;67:433–447.
36. Moretti P, Bouwknecht JA, Teague R, Paylor R, Zoghbi HY. Abnormalities of social interactions and home-cage behavior in a mouse model of Rett syndrome. *Hum Mol Genet.* 2005;14:205–220.
37. Barker MS, Manoochehri M, Rizer SJ, et al. Recognition memory and divergent cognitive profiles in prodromal genetic frontotemporal dementia. *Cortex.* 2021;139:99–115.
38. Blass DM, Rabins PV. Depression in frontotemporal dementia. *Psychosomatics.* 2009;50:239–247.
39. Kalueff AV, Stewart AM, Song C, Berridge KC, Graybiel AM, Fentress JC. Neurobiology of rodent self-grooming and its value for translational neuroscience. *Nat Rev Neurosci.* 2016;17:45–59.
40. Sturman O, Germain PL, Bohacek J. Exploratory rearing: A context- and stress-sensitive behavior recorded in the open-field test. *Stress.* 2018;21:443–452.
41. Zimprich A, Garrett L, Deussing JM, et al. A robust and reliable non-invasive test for stress responsivity in mice. *Front Behav Neurosci.* 2014;8:125.
42. Fuzesi T, Daviu N, Wamsteeker Cusulin JI, Bonin RP, Bains JS. Hypothalamic CRH neurons orchestrate complex behaviours after stress. *Nat Commun.* 2016;7:11937.
43. Premoli M, Pietropaolo S, Wohr M, Simola N, Bonini SA. Mouse and rat ultrasonic vocalizations in neuroscience and neuropharmacology: State of the art and future applications. *Eur J Neurosci.* 2023;57:2062–2096.
44. Semple BD, Noble-Haesslein LJ, Jun Kwon Y, et al. Sociosexual and communication deficits after traumatic injury to the developing murine brain. *PLoS One.* 2014;9:e103386.
45. Burke K, Ohman KA, Manohar S, Dent ML. Blast trauma affects production and perception of mouse ultrasonic vocalizations. *J Acoust Soc Am.* 2022;151:817.
46. Menuet C, Cazals Y, Gestreau C, et al. Age-related impairment of ultrasonic vocalization in Tau.P301L mice: Possible implication for progressive language disorders. *PLoS One.* 2011;6:e25770.
47. Siebzehnruhl FA, Raber KA, Urbach YK, et al. Early postnatal behavioral, cellular, and molecular changes in models of Huntington disease are reversible by HDAC inhibition. *Proc Natl Acad Sci U S A.* 2018;115:E8765–E8774.
48. Graham NS, Sharp DJ. Understanding neurodegeneration after traumatic brain injury: From mechanisms to clinical trials in dementia. *J Neurol Neurosurg Psychiatry.* 2019;90:1221–1233.
49. Liu Y, Pattamatta A, Zu T, et al. C9orf72 BAC mouse model with motor deficits and neurodegenerative features of ALS/FTD. *Neuron.* 2016;90:521–534.
50. Riemsdijk FW, van der Toorn EC, Verhagen RFM, et al. Inducible expression of human C9ORF72 36x G4C2 hexanucleotide repeats is sufficient to cause RAN translation and rapid muscular atrophy in mice. *Dis Models Mech.* 2021;14:dmm044842.
51. Starr A, Sattler R. Synaptic dysfunction and altered excitability in C9ORF72 ALS/FTD. *Brain Res.* 2018;1693(Pt A):98–108.
52. Jamjoom AAB, Rhodes J, Andrews PJD, Grant SGN. The synapse in traumatic brain injury. *Brain.* 2021;144:18–31.
53. Han SP, Tang YH, Smith R. Functional diversity of the hnRNPs: Past, present and perspectives. *Biochem J.* 2010;430:379–392.
54. Polymenidou M, Lagier-Tourenne C, Hutt KR, et al. Long pre-mRNA depletion and RNA missplicing contribute to neuronal vulnerability from loss of TDP-43. *Nat Neurosci.* 2011;14:459–468.
55. Tollervey JR, Curk T, Rogelj B, et al. Characterizing the RNA targets and position-dependent splicing regulation by TDP-43. *Nat Neurosci.* 2011;14:452–458.
56. Dyer MS, Woodhouse A, Blizzard CA. Cytoplasmic human TDP-43 mislocalization induces widespread dendritic spine loss in mouse upper motor neurons. *Brain Sci.* 2021;11:883.
57. Cooper-Knock J, Hewitt C, Highley JR, et al. Clinico-pathological features in amyotrophic lateral sclerosis with expansions in C9ORF72. *Brain.* 2012;135(Pt 3):751–764.
58. Liu G, Ou S, Cui H, et al. Head injury and amyotrophic lateral sclerosis: A meta-analysis. *Neuroepidemiology.* 2021;55:11–19.
59. Mackenzie IR, Arzberger T, Kremmer E, et al. Dipeptide repeat protein pathology in C9ORF72 mutation cases: Clinicopathological correlations. *Acta Neuropathol.* 2013;126:859–879.
60. Anderson EN, Gochenaur L, Singh A, et al. Traumatic injury induces stress granule formation and enhances motor dysfunctions in ALS/FTD models. *Hum Mol Genet.* 2018;27:1366–1381.
61. Anderson EN, Morera AA, Kour S, et al. Traumatic injury compromises nucleocytoplasmic transport and leads to TDP-43 pathology. *Elife.* 2021;10:e67587.
62. Katzenberger RJ, Loewen CA, Wassarman DR, Petersen AJ, Ganetzky B, Wassarman DA. A Drosophila model of closed head traumatic brain injury. *Proc Natl Acad Sci U S A.* 2013;110:E4152–E4159.
63. Alkaslasi MR, Cho NE, Dhillon NK, et al. Poor corticospinal motor neuron health is associated with increased symptom severity in the acute phase following repetitive mild TBI and predicts early ALS onset in genetically predisposed rodents. *Brain Sci.* 2021;11:160.

64. Thomsen GM, Vit JP, Lamb A, et al. Acute traumatic brain injury does not exacerbate amyotrophic lateral sclerosis in the SOD1 (G93A) rat model. *eNeuro*. 2015;2:ENEURO.0059-14.2015.
65. Evans TM, Jaramillo CA, Sataranatarajan K, et al. The effect of mild traumatic brain injury on peripheral nervous system pathology in wild-type mice and the G93A mutant mouse model of motor neuron disease. *Neuroscience*. 2015;298:410-423.
66. Thomsen GM, Ma AM, Ko A, et al. A model of recurrent concussion that leads to long-term motor deficits, CTE-like tauopathy and exacerbation of an ALS phenotype. *J Trauma Acute Care Surg*. 2016;81:1070-1079.
67. Martin LJ, Wong M, Hanaford A. Neonatal brain injury and genetic causes of adult-onset neurodegenerative disease in mice interact with effects on acute and late outcomes. *Front Neurol*. 2019;10:635.
68. Kim RB, Irvin CW, Tilva KR, Mitchell CS. State of the field: An informatics-based systematic review of the SOD1-G93A amyotrophic lateral sclerosis transgenic mouse model. *Amyotroph Lateral Scler Frontotemporal Degener*. 2015;17(1-2):1-14.
69. Kahrman A, Bouley J, Bosco DA, Shazeeb MS, Henninger N. Differential association of baseline body weight and body-weight loss with neurological deficits, histology, and death after repetitive closed head traumatic brain injury. *Neurosci Lett*. 2022;771:136430.
70. Ghasemi M, Keyhanian K, Douthwright C. Glial cell dysfunction in C9orf72-related amyotrophic lateral sclerosis and frontotemporal dementia. *Cells*. 2021;10:249.
71. Zhang J, Velmeshev D, Hashimoto K, et al. Neurotoxic microglia promote TDP-43 proteinopathy in progranulin deficiency. *Nature*. 2020;588:459-465.
72. Klim JR, Pintacuda G, Nash LA, Guerra San Juan I, Eggen K. Connecting TDP-43 pathology with neuropathy. *Trends Neurosci*. 2021;44:424-440.
73. Klim JR, Williams LA, Limone F, et al. ALS-implicated protein TDP-43 sustains levels of STMN2, a mediator of motor neuron growth and repair. *Nat Neurosci*. 2019;22:167-179.
74. Melamed Z, Lopez-Erauskin J, Baughn MW, et al. Premature polyadenylation-mediated loss of stathmin-2 is a hallmark of TDP-43-dependent neurodegeneration. *Nat Neurosci*. 2019;22:180-190.
75. Tran H, Moazami MP, Yang H, et al. Suppression of mutant C9orf72 expression by a potent mixed backbone antisense oligonucleotide. *Nat Med*. 2022;28:117-124.
76. Meijboom KE, Abdallah A, Fordham NP, et al. CRISPR/Cas9-mediated excision of ALS/FTD-causing hexanucleotide repeat expansion in C9ORF72 rescues major disease mechanisms in vivo and in vitro. *Nat Commun*. 2022;13:6286.
77. Cook CN, Wu Y, Odeh HM, et al. C9orf72 poly(GR) aggregation induces TDP-43 proteinopathy. *Sci Transl Med*. 2020;12:eabb3774.
78. Wang Y, Liu Y, Nham A, et al. Calpain-2 as a therapeutic target in repeated concussion-induced neuropathy and behavioral impairment. *Sci Adv*. 2020;6:eaba5547.